SIGNALS FROM A BEAM PERFORMING BETATRON OSCILLATIONS USING AN ELECTROSTATIC ELECTRODE MODEL WITH RECTANGULAR BOUNDARIES

F. Nolden, GSI, Darmstadt, Germany
J.X. Wu, IMP, Lanzhou, China

Abstract

We investigate the non-linear response of a pick-up structure using electrostatic models with the formalism introduced by Bisognano and Leeman. As an example we show results from the pick-up structure at the CSRe storage ring at the IMP in Lanzhou.

ELECTROSTATIC MODELS OF AN ELECTRODE PLATE

Electrostatic Models of Relativistic Beam Response

Electrostatic models have been applied for a long time to the investigation of the response of both pick-ups and kickers. A classical overview of this subject is due to G. Lambertson [1]. He gives also an equation of the non-relativistic case, but this is meant to show that the electrostatic approximation is good for large Lorentz factors γ.

A more naive approach to the non-relativistic case is to replace the extremely short field disk of ultra-relativistic particles by the correct expressions for a free particle [2, 3]. This leads to analytical expressions of the correction, however the boundary conditions of a real vacuum chamber are not taken into account.

As this paper mainly aims at a study of the response to betatron oscillations, the electrostatic approximation is used throughout.

Parallel Boundaries without Borders

The electrostatic model with parallel boundaries was first introduced by Neuffer [4]. The underlying conformal mapping is explained in some detail in [3]. However we use here a different coordinate system where the y coordinate is zero in the center of the vacuum chamber (see Fig. 1).

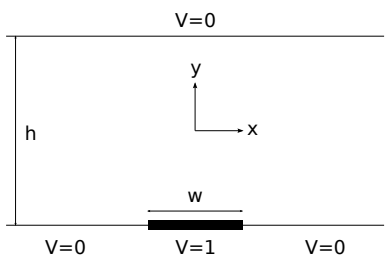

Figure 1: Electrode with parallel boundaries

The model can be calculated as follows. Take

$$z = \frac{\cos(\pi y/h)\sinh(\pi w/2h)}{\cosh(\pi x/h) + \sin(\pi y/h)\cosh(\pi w/2h)} \qquad (1)$$

where w is the width of one electrode and h is the height of the chamber.

$$S(x,y) = \begin{cases} \frac{1}{\pi}\arctan z & \text{if} \quad z > 0 \\ 0.5 & \text{if} \quad z = 0 \\ 1 + \frac{1}{\pi}\arctan z & \text{if} \quad z < 0 \end{cases} \qquad (2)$$

The case distinction is necessary because one has to switch between Riemann sheets of the inverse tangent function in order to get an analytic potential. The third case occurs if the point (x, y) gets vertically close to the electrode.

Rectangular Borders

To model a rectangular chamber requires a slightly more complicated conformal mapping.

A rectangular chamber in the $z = x - y$-plane extends from $-a/2$ to $a/2$ in x and from 0 to b in y (see Fig. 2). A potential V is supposed to exist from x_1 to x_2 along the x-axis.

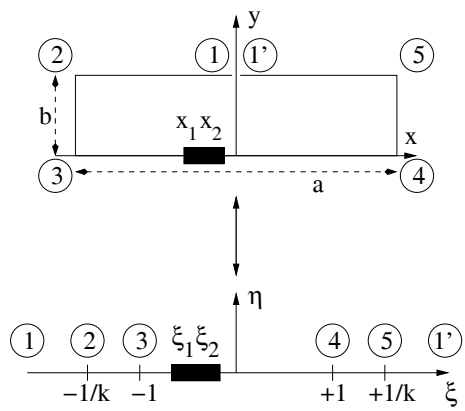

Figure 2: Conformal mapping of inner part of a rectangle to the upper half plane ($k^2 = m$).

The potential is calculated after a conformal mapping of the interiour of the rectangle to the upper complex half-plane.

$$z = x + iy \;\mapsto\; \zeta = \xi + i\eta \qquad (3)$$

Such a mapping can be realized by [5]

$$\zeta = \mathrm{sn}\left(\frac{2K(m)}{a} z|m\right) \qquad (4)$$

where sn is one of the Jacobian elliptic functions (using the notation from [6]) and K is a complete elliptic integral of the first kind. The parameter m depends on the aspect ratio a/b of the rectangle. It solves the equation [5]

$$\frac{a}{b} - \frac{2K(m)}{K(1-m)} = 0 \qquad (5)$$

ISBN 978-3-95450-174-8

which is due to the periods $4K(m)$ and $2iK(1-m)$ of the doubly periodic function $\mathrm{sn}(z|m)$ (see [6]).

The Jacobian elliptic functions of a complex argument are calculated from real arguments using (see [6])

$$\mathrm{sn}(x+iy|m) = \frac{s\,d_1 + i\,c\,d\,s_1\,c_1}{c_1^2 + m\,s^2\,s_1^2} \tag{6}$$

where

$$\begin{aligned} s &= \mathrm{sn}(x|m), \quad & s_1 &= \mathrm{sn}(y|1-m) \\ c &= \mathrm{cn}(x|m), \quad & c_1 &= \mathrm{cn}(y|1-m) \\ d &= \mathrm{dn}(x|m), \quad & d_1 &= \mathrm{dn}(y|1-m) \end{aligned} \tag{7}$$

and where cn and dn are also Jacobian elliptic functions.

In order to calculate the potential at a point (x, y), one maps $z = x + iy \mapsto \zeta$ and gets the physical potential V as the real part of

$$\Phi(\zeta) = \frac{i}{\pi} \log\left[\frac{\zeta - \xi_2}{\zeta - \xi_1}\right] \tag{8}$$

where the edges of the electrode are mapped according to $(x_{12}, 0) \mapsto (\xi_{12}, 0)$.

This gives rise to using an inverse tangent function, because

$$\mathrm{Im}\left[\log(u+iv)\right] = \arctan\frac{v}{u} \tag{9}$$

The Riemann sheets of the inverse tangent are chosen in exactly the same way as in Eq. (2).

NON-LINEAR RESPONSE FORMALISM

In the case of betatron motion, the particle coordinates at the pick-up oscillate:

$$x_n = x_\delta + A_x \sin\alpha_{x,n} \tag{10}$$

$$y_n = A_y \sin\alpha_{y,n} \tag{11}$$

where $x_\delta = D\delta p/p$ is a dispersive offset, and $A_{x,y} = \sqrt{\epsilon_{x,y}\beta_{x,y}}$ are the betatron amplitudes calculated in the usual way from the one-particle emittances $\epsilon_{x,y}$ and the betatron functions $\beta_{x,y}$. The betatron angles

$$\alpha_{y,n} = 2\pi n Q_{xy} + \mu_{x,y} \tag{12}$$

where Q_{xy} is the number of betatron oscillations per turn and $\mu_{x,y}$ is an initial phase.

To deal with the oscillating particle positions, Bisognano and Leeman [7] proposed the following elegant formalism:

Make a wave number decomposition of $S(x, y)$, i.e. introduce the 2D Fourier transform

$$\tilde{S}(k_x, k_y) = \iint_{\mathbb{R}^2} dx\,dy\; S(x,y) e^{-i(k_x x + k_y y)} \tag{13}$$

Transforming backwards yields

$$S(x,y) = \frac{1}{(2\pi)^2} \iint_{\mathbb{R}^2} dk_x\,dk_y\; \tilde{S}(k_x,k_y) e^{+i(k_x x + k_y y)} \tag{14}$$

where the coordinates x, y now appear only in the exponential. With the Bessel function expansion

$$e^{+ik_x x_n} = e^{+ik_x x_\delta} \sum_{l_x=-\infty}^{\infty} J_{l_x}(k_x A_x) e^{+il_x\alpha_x} \tag{15}$$

$$e^{+ik_y y_n} = \sum_{l_y=-\infty}^{\infty} J_{l_y}(k_y A_y) e^{+il_y\alpha_y} \tag{16}$$

one can therefore write, after reversing the order of sums and integrals:

$$S(x_n, y_n) = \sum_{l_x-\infty}^{\infty} \sum_{l_y-\infty}^{\infty} S_{l_x,l_y}(A_x, A_y, x_\delta) e^{+i(l_x\alpha_x + l_y\alpha_y)} \tag{17}$$

with the coefficients

$$\begin{aligned} S_{l_x,l_y}(A_x, A_y, x_\delta) &= \frac{1}{(2\pi)^2} \iint_{\mathbb{R}^2} dx\,dy\; \tilde{S}(k_x,k_y) \\ &\times J_{l_x}(k_x A_x) J_{l_y}(k_y A_y) e^{+ik_x x_\delta} \end{aligned} \tag{18}$$

Using Eq. (10), Eq. (11) it can be shown [3] that the response of a pick-up yields generally a signal at the frequencies

$$\omega(m, l_x, l_y) = \left(m + l_x Q_x + l_y Q_y\right)\omega_{\mathrm{rev}} \tag{19}$$

where ω_{rev} is the particle revolution frequency. Which of these frequencies dominate, depends on the construction of the pick-up and on the betatron amplitudes. Large signals are usually detected only at the central harmonics ($l_x = l_y = 0$) and at the betatron sidebands ($|l_x| = 1$ and $|l_y| = 1$).

Particularly important is the case of small betatron amplitudes $A_{x,y}$. Then one can can use the appromixations $J_0(z) \approx 1$, and $J_1(z) \approx z/2$. One gets

$$S_{0,0} \approx S(x_\delta, y) \tag{20}$$

$$S_{1,0} \approx \frac{A_x}{2i}\frac{\partial S(x_\delta, y)}{\partial x} \tag{21}$$

$$S_{0,1} \approx \frac{A_y}{2i}\frac{\partial S(x_\delta, y)}{\partial y} \tag{22}$$

A more detailed discussion is given in [3, 7].

SIMULATION RESULTS FOR CSRE STOCHASTIC COOLING

Electrode Geometry

Presently a stochastic cooling system is being installed at the CSRe storage ring at the Institute of Modern Physics in Lanzhou, China [8]. Three pick-up and kicker systems have been installed which all share the same transverse geometry [9].

The pick-up (Fig. 3) consists of four equal electrodes with $w = 87$ mm and $h = 62$ mm (using the notation of Fig. 1). The electrodes are arranged symmetrically with respect to the center of the vacuum chamber. The horizontal distance from the center to the center of each electrode is 57.5 mm.

ISBN 978-3-95450-174-8

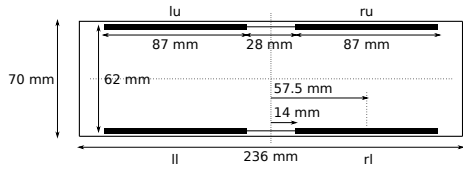

Figure 3: Geometry of CSRe electrodes.

We denote the different electrodes with the symbols *lu* (left upper), *ll* (left lower), *ru* (right upper), and *rl* (right lower). The signals of each single electrodes can be processed in three different modes:

1. The sum mode (symbollically $lu + ll + ru + rl$). This mode can be used for longitudinal cooling (time of flight or notch filter).

2. The horizontal difference mode (symbollically $lu + ll - ru - rl$). This mode can be used for longitudinal cooling (Palmer) and for horizontal betatron cooling.

3. The vertical difference mode (symbollically $lu - ll + ru - rl$). This mode can be used for vertical betatron cooling.

Sum Mode

Figure 4 shows the case if the sum from all four electrodes is taken. We examine this case in some detail.

Each curve in Fig. 4 shows the sensitivity as a function of x for fixed y. The different curves are plotted for different values of the vertical coordinate y. For $x = y = 0$ the value of the sensitivity is $S \approx 0.58$. Towards the middle of the plates $(x, y) = (\pm 57.5\,\text{mm}, 0\,\text{mm})$ it rises on both sides to $S \approx 0.85$ and drops steeply to 0 towards higher values of $|x|$. At $x = 0$ the sensitivity drops rapidly to 0 if the verical position approaches the $V = 0$ position in the gap between the plates. On the other hand it gets close to 1 in the vicinity of the plates.

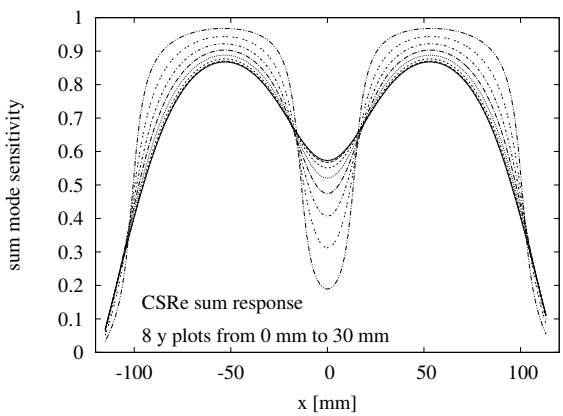

Figure 4: CSRe sum response.

Figure 5 shows the sensitivity $S_{0,0}$ (central revolution frequency harmonics) for a particle with $x_\delta = 0\,\text{mm}$ performing betatron oscillations with various amplitudes A_x and A_y. Each curve is plotted for fixed A_y and 16 curves are plotted for $0\,\text{mm} \leq A_y \leq 30\,\text{mm}$.

As to be expected the sensitivity for zero amplitudes is $S \approx 0.58$. As a function of A_x the sensitivity rises until the betatron amplitude is slightly larger than 57.5 mm. For very small horizontal amplitudes A_x, the sensitivity decreases for large A_y, but for $A_x \approx 35\,\text{mm}$ a point is reached where $S_{0,0}$ becomes roughly independent of A_y.

As a practical consequence of such considerations, it might be too naive to derive the number of particles in a beam from the area in the Schottky spectra, if they are measured at significantly different transverse emittances.

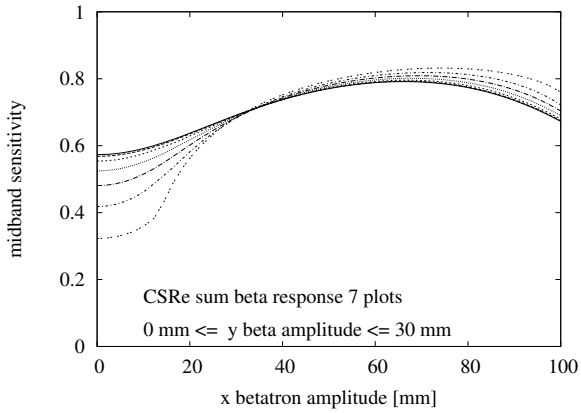

Figure 5: CSRe response to betatron oscillations in sum mode.

Horizontal Difference Mode

Figure 6 shows the response in the horizontal difference mode. The plot is made in the same way as Fig. 4. The horizontal response is more or less linear up to $|x| \approx 40mm$ and the dependence on y becomes predominant only in the vicinity of the plates.

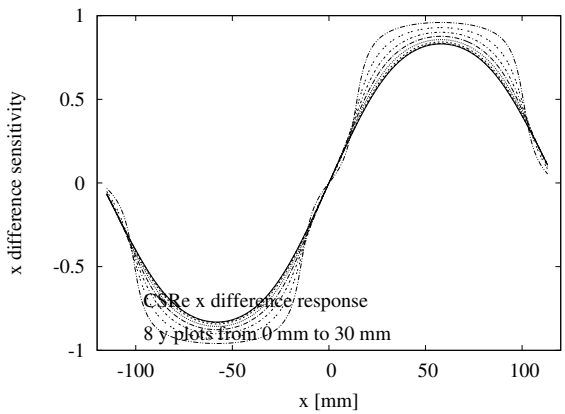

Figure 6: CSRe horizontal difference response.

Figure 7 shows the response $S_{1,0}$ in the same way as Fig. 5. The linearity in A_x is very good for small amplitudes and the dependence on A_y is almost negligible.

ISBN 978-3-95450-174-8

Curves like these can also be used to verify the approximation Eq. (21).

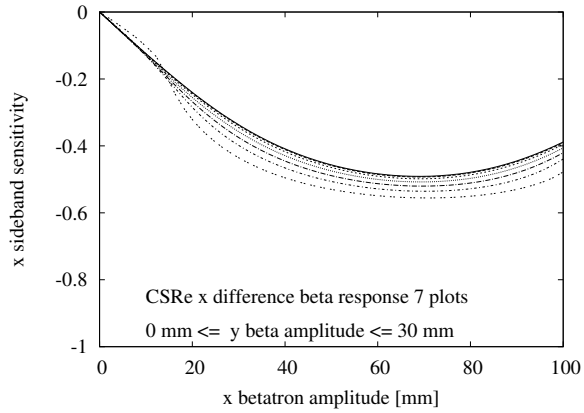

Figure 7: CSRe response to betatron oscillations in horizontal difference mode.

Vertical Difference Mode

Figure 8 shows the response in the vertical difference mode. The plot is made in the same way as Figure 4 At $x = 0\,\text{mm}$ the sensitivity does not exceed $|S| \approx 0.15$. Whereas it is approximately linear in y in the vicinity of the plates (for $|x| \approx 57.5\,\text{mm}$), there is a maximum at $y \approx 16\,\text{mm}$, if $x \lessapprox 20\,\text{mm}$.

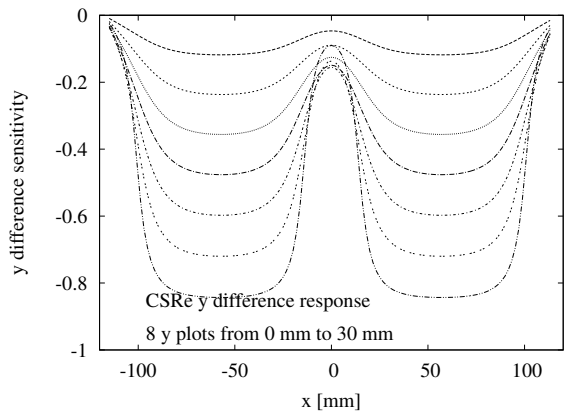

Figure 8: CSRe vertical difference response

Figure 9 shows the response $S_{0,1}$ in the same way as Figure 5.

The nonlinearity for $x \gtrapprox 20\,\text{mm}$ mentioned above is also clearly visible in the $S_{0,1}$ response. As a result it might be argued that pick-ups with a horizontal gap in the middle are not ideally suited for vertical betatron cooling.

CONCLUSIONS

It has been shown that the non-linear response formalism yields detailed informations on the response of electrode structures to particles performing betatron oscillations.

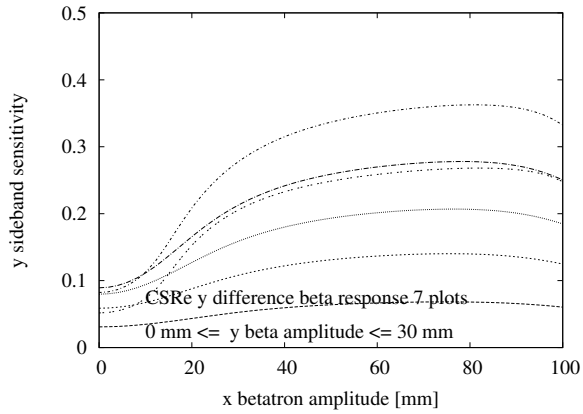

Figure 9: CSRe response to betatron oscillations in vertical difference mode

It is straightforward to implement it on a computer using digital Fourier transform techniques.

It is recommended to use it as a valuable tool for electrode design.

REFERENCES

[1] G. Lambertson, in Physics of High Energy Accelerators, SLAC Summer School 1985, Fermilab Summer School 1984, AIP Conf. Proc. 153, pp. 1413–1442, (1984).

[2] F. Caspers, G. Dôme, Reciprocity between Pick-up and Kicker Structures Including the Far-Field Zone, Proc. EPAC 1994, pp. 1208–1210, (1994).

[3] F. Nolden, Stochastic Cooling and Related RF Components, in CERN Accelerator School on RF Engineering, CERN Yellow Report 2005-003, pp. 400–420, (2005).

[4] D. Neuffer, Fermilab pbar note 201, (1982).

[5] E. Durand, Electrostatique, Tôme II (Problèmes généraux conducteurs), Masson (Paris), (1966).

[6] M. Abramovitz, I. Stegun, Handbook of Mathematical Functions, National Bureau of Standards Applied Mathematics Series 55, (1972).

[7] J. Bisognano, C. Leemann, in Physics of High Energy Accelerators, Fermilab School 1981, AIP Conf. Proc. **87**, (1982).

[8] J.X. Wu et al., Stochastic Cooling Project at the Experimental Storage Ring CSRe at IMP, Proc. of Cool'11, pp. 64–66, (2011).

[9] Y. Zhang et al., An Improved Forward Travelling Wave Structure Design For Stochastic Cooling at Experimental Storage Ring (CSRe) at the Institute of Modern Physics (IMP) in China, Proc. of Cool'11, pp. 132–135, (2011).

ISBN 978-3-95450-174-8